THE JOURNAL OF PHYSICAL CHEMISTRY B

Article

pubs.acs.org/JPCB

Structural Changes and Aggregation Mechanisms for Anti-Streptavidin IgG1 at Elevated Concentration

Gregory V. Barnett,[†] Wei Qi,[‡] Samiul Amin,[‡] E. Neil Lewis,[‡] Vladimir I. Razinkov,[§] Bruce A. Kerwin,[§,∥] Yun Liu,[†,⊥] and Christopher J. Roberts*[,†]

[†]Department of Chemical and Biomolecular Engineering, University of Delaware, Newark, Delaware 19716, United States

[‡]Malvern Biosciences Incorporated, Columbia, Maryland 21046, United States

[§]Drug Product Development, Amgen Incorporated, Seattle, Washington 98119, United States

[⊥]Center for Neutron Science, National Institutes of Standards and Technology, Gaithersburg, Maryland 20899, United States

Supporting Information

ABSTRACT: Non-native protein aggregation may occur during manufacturing and storage of protein therapeutics, and this may decrease drug efficacy or jeopardize patient safety. From a regulatory perspective, changes in higher order structure due to aggregation are of particular interest but can be difficult to monitor directly at elevated protein concentrations. The present report focuses on non-native aggregation of antistreptavidin (AS) IgG1 at 30 mg/mL under solution conditions that prior work at dilute concentrations (e.g., 1 mg/mL) indicated would result in different aggregation mechanisms. Time-dependent aggregation and structural changes were monitored in situ with dynamic light scattering, small-angle neutron scattering, and Raman scattering and ex situ with far-UV circular dichroism and second-derivative UV spectroscopy. The effects of adding 0.15 M (~5 w/w %) sucrose were also assessed. The addition of sucrose decreased monomer loss rates but did not change protein−protein interactions, aggregation mechanism(s), or aggregate structure and morphology. Consistent with prior results, altering the pD or salt concentration had the primary effect of changing the aggregation mechanism. Overall, the results provide a comparison of aggregate structure and morphology created via different growth mechanisms using orthogonal techniques and show that the techniques agree at least qualitatively. Interestingly, AS-IgG1 aggregates created at pD 5.3 with no added salt formed the smallest aggregates but had the largest structural changes compared to other solution conditions. The observation that the larger aggregates were also those with less structural perturbation compared to folded AS-IgG1 might be expected to extend to other proteins if the same strong electrostatic repulsions that mediate aggregate growth also mediate structural changes of the constituent proteins within aggregates.

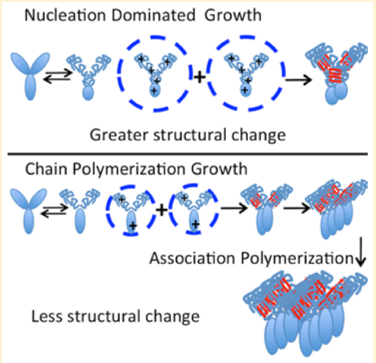

INTRODUCTION

Monoclonal antibodies (mAbs) are one of the fastest growing classes of drug candidates in the biopharmaceutical industry. Currently, there are over 39 mAbs on the market in the United States or European Union, and hundreds of these molecules are being developed in biopharmaceutical pipelines.[1] mAbs offer treatment for many chronic or fatal diseases, such as cancers and autoimmune diseases. Unwanted immunogenicity is a potential side effect associated with protein-based therapeutics.[2,3] As such, a patient's immune system may register the therapeutic as a potential threat and mount an immune response. Unfortunately, predicting if and when immunogenicity may occur is challenging, as there are many possible patient-related factors and drug quality attributes that may contribute to this issue.[4,5]

Product purity is arguably the largest factor affecting immunogenicity. For instance, heterogeneities in the primary sequence of the protein as well as glycosylation patterns have been linked to immunogenicity.[6] Foreign particulates, such as silicone oils from fill-finish processes, as well as proteinaceous particles, such as protein aggregates, may also contribute to immunogenicity.[7,8] In this context, a non-native protein aggregate is defined as a net irreversible cluster of protein monomers that have lost some or all of their native (folded) structure. Non-native aggregates (hereafter referred to as aggregates) may still retain a significant fraction of native structure in the constituent protein chains and can be one of the most difficult degradation processes to control and/or predict during manufacturing and storage.

Larger sized aggregates and higher concentration of aggregates are factors that have been shown to increase immunogenicity.[3,4] Additionally, aggregates that display epitopes or repeating structures within the aggregate that are similar to therapeutically active protein may elicit antidrug antibodies and render future treatments ineffective.[9] As such, understanding the mechanism(s) by which aggregates form and

Received: September 7, 2015
Revised: October 28, 2015
Published: November 12, 2015

DOI: 10.1021/acs.jpcb.5b08748
J. Phys. Chem. B 2015, 119, 15150−15163

monitoring their morphology and structure may help assess immunogenic risk of a therapeutic protein.

Typical dosing requirements for mAb treatments range from 100 to 200 mg, and if administered as a single subcutaneous injection, the protein concentration can easily reach larger than 100 mg/mL.[10] At elevated protein concentrations, nonideal protein−protein interactions may give rise to increases in solution viscosity[10−12] or accelerate degradation rates such as aggregation.[13] Monitoring protein structure and aggregate morphology at intermediate to high protein concentrations is challenging, as many analytical techniques are limited to low protein concentration.[10] This forces many techniques to be employed after diluting samples to work properly within instrumental limits. Aggregation is often monitored with ex-situ techniques that inherently suffer from these limitations, e.g., chromatography with inline scattering,[14,15] microflow imaging,[16,17] and nanoparticle tracking.[18,19] Relatively little has been reported for monitoring in-situ aggregation of mAb-based systems at high or low concentrations or for comparing structural changes from in-situ and ex-situ methods.[20]

Previous work has highlighted that the underlying aggregation mechanisms dictate the net aggregate concentration(s) and size distribution and potentially also the residual protein structure within resulting aggregates.[21] Aggregation involves partial or full unfolding of the protein, which disrupts the secondary and tertiary structure and putatively exposes hydrophobic patches.[22] Aggregates are often stabilized by intermolecular β-sheet contacts between (partially) unfolded proteins.[23] Because mAbs are large, multidomain proteins, it is possible that only one of the domains needs to be (partially) unfolded in order for aggregates to form.[24−26]

Under some solution conditions, aggregates of immunoglobulin gamma-1 (IgG1) have been shown to have little growth beyond nucleation or initiation of the smallest aggregates (e.g., dimers), and this mechanism has been termed nucleation-dominated (ND) aggregation.[27] Aggregates may also grow by chain polymerization (CP), by which partially unfolded monomers add directly to existing aggregates. Additionally, association polymerization (AP) may occur, in which an aggregate may coalesce with another aggregate to form a larger species. However, AP growth occurs with significant rates only once a sufficiently high concentration of aggregates has been achieved. This follows because AP does not involve monomeric protein, which is the dominant species at the start of the aggregation process for most therapeutic proteins.[28] While prior work has focused primarily on categorizing aggregate mechanisms based on how the average aggregate molecular weight changes as the process proceeds, it remains unclear if the underlying structure and aggregate morphology must also change as one changes solution conditions to mediate aggregate growth mechanism(s).[25,29]

It is anticipated that the underlying aggregate structure may be different for aggregates created by different "stresses". For example, IgG dimers created through different "stresses" (i.e., heating, UV exposure, stirring, etc.) resulted in different aggregate morphologies.[30] Similarly, it has been shown elsewhere that different stresses may affect the immunogenicity of the resulting samples.[31] Prior work suggested that different aggregation mechanisms in solution may lead to different secondary structure(s) in the constituent protein chains.[32−34] Kim et al. reported increased antiparallel β-sheet content for IgG1 aggregation via the ND mechanism when compared to CP or AP mechanisms at low protein concentration.[25] However, recent results have also suggested that IgG1 aggregation at higher protein concentrations (e.g., ∼100 mg/mL) may occur first through native, reversible complexes that then unfold/rearrange to form irreversible aggregates, because the elevated protein concentration promotes weak but non-negligible native self-association.[35−37] Ex-situ measurements cannot discern between a mechanism in which unfolding occurs prior to self-association rather than after it. Therefore, monitoring aggregation via in-situ measurements at elevated protein concentrations may provide insights into aggregation mechanisms that may be less kinetically important at lower protein concentrations.

This report provides a systematic characterization of antistreptavidin IgG1 (AS-IgG1) aggregation at an intermediate protein concentration (30 mg/mL). Aggregate morphology and structure were monitored for solution conditions that promote ND, CP, or AP growth mechanisms in the presence and absence of sucrose using a series of complementary techniques. Structural changes during aggregation were monitored ex situ with traditional techniques, circular dichroism, and UV absorption. In-situ aggregation was monitored with a combination of dynamic light scattering, Raman scattering, and small-angle neutron scattering (SANS); these were also compared with ex-situ laser light scattering. The results highlight the effects of pD and NaCl on the growth mechanism. Raman, CD, and second-derivative UV suggest larger structural perturbation for aggregates created via the ND mechanism compared to those created with the CP or CP/AP mechanism. The addition of sucrose decreases aggregation rates rather than altering protein−protein interactions or growth mechanisms. Together these results highlight advantages and disadvantages of monitoring aggregation in situ vs ex situ at elevated protein concentrations.

MATERIALS AND METHODS

Sample Preparation. AS-IgG1 stock solution at ∼30 mg/mL was provided by Amgen. All solutions were buffer exchanged into deuterium oxide (D_2O) (99% D atom, Sigma Aldrich) solutions. Buffers were prepared in 10 mM acetic acid (Fisher Scientific) and in some cases with the addition of 100 mM NaCl (Fisher Scientific) and/or 0.15 M sucrose (>99.5% (HPLC grade), Sigma Aldrich). Solutions were adjusted to the desired pD with 1 M sodium hydroxide (Fisher Scientific) stock solution in D_2O using the standard expression (eq 1), which relates the pD value to pH*, the apparent pH value read from the instrument.[38]

$$pD = pH^* + 0.4 \quad (1)$$

Each protein solution was buffer exchanged with its corresponding buffer using Amicon centrifuge tubes (Millipore, Billerica, MA) a minimum of four times. Following buffer exchange, the protein concentration was determined from absorbance at 280 nm using a UV−vis spectrometer (Agilent 8453 UV−vis, Agilent Technologies, Santa Clara, CA) with an extinction coefficient of 1.586 mL/mg cm for AS-IgG1. All solutions were prepared gravimetrically, and the final protein concentration and pD were checked and reported in solution conditions below.

Ex-Situ Monomer Loss Kinetics and Light Scattering Using SEC-MALS. Solutions were prepared in the following solution conditions based on prior published results: pD 5.3 and 10 mM acetate; pD 4.6 with 100 mM NaCl and 10 mM acetate; and pD 5.1 with 100 mM NaCl and 10 mM acetate.[29]

DOI: 10.1021/acs.jpcb.5b08748
J. Phys. Chem. B 2015, 119, 15150−15163

The final protein concentration was 30 mg/mL in all cases. Solutions with the same conditions as above but also containing 0.15 M sucrose were also prepared. Aliquots of each protein solution were placed into HPLC vials (Waters, Milford, MA) and hermetically sealed before incubation. Vials were heated isothermally, and at a series of preselected time points, vials were quenched in an ice bath to arrest aggregation.

Quenched protein solutions were diluted to a final concentration of 0.5−1.5 mg/mL and left at room temperature (20−23 °C) before injecting onto the HPLC. For each diluted protein solution, the monomer fraction and molecular weight where determined with size exclusion chromatography with in-line multiangle light scattering (SEC-MALS). Each protein solution was injected using an autosampler on an Agilent 1100 HPLC (Agilent Technologies, Santa Clara, CA), and the monomer was separated from aggregate population using a Tosoh (Montgomeryville, PA) TSK-Gel 3000xL size exclusion column. Following the SEC column, the absorbance at 280 nm was measured using a variable wavelength detector (VWD, Agilent Technologies), which recorded the absorbance of the eluting monomer and aggregate peaks. The monomer fraction remaining (m) is defined as the monomer peak area relative to that for an unheated protein solution and was calculated for each injection as previously reported.[39] A multiangle-light-scattering (MALS) instrument, DAWN-HELEOS II (Wyatt Technologies, Santa Barbara, CA), was used inline following the VWD and recorded static and dynamic light scattering from the eluting monomer and aggregate peaks. The total molecular weight (M_w^{tot}) was determined using ASTRA VI software as previously described.[14]

Circular Dichroism. Quenched protein solutions were diluted to 0.5 mg/mL, and far-UV circular dichroism (CD) spectra were recorded using a Jasco J-810 spectrophotometer (Jasco, Easton, MD) at 25 °C. CD spectra were measured from 200 to 250 nm at a scan rate of 20 nm/min using 1 × 10 mm Hellma cuvettes (Plainview, NY). Ten spectra were collected and averaged for each measurement. As previously described, the buffer spectrum was subtracted and the mean residue ellipticity, $[\theta]$, was calculated using the standard expression.[40] Using the known monomer fraction (m) the monomer contribution to a given CD spectrum was subtracted at a given wavelength by subtracting the product of m and the measured CD spectra for a pure monomeric solution $[\theta_m]$ via eqs 2a and 2b as previously described.[39,41] The net aggregate contribution to the measured ellipticity for a given sample, $[\theta_{agg}]$, was calculated from eqs 2a and 2b for each wavelength. This analysis allows one to distinguish between changes in spectra that are due to different amounts of monomer present for samples that are incubated for different times to promote aggregation. In eqs 2a and 2b, m depends only on the incubation time for given solution conditions, while the ellipticity values depend on both time and wavelength.

$$[\theta] = [\theta_m]m + (1 - m)[\theta_{agg}] \tag{2a}$$

$$[\theta_{agg}] = \frac{[\theta] - m[\theta_m]}{(1 - m)} \tag{2b}$$

Second-Derivative UV Absorption. Quenched samples were diluted to 1.5−2 mg/mL, and the absorbance spectra from 200 to 400 nm were recorded using a UV−vis spectrometer with a photodiode array (Agilent Technologies). Spectra were collected over a 1 s integration time using a 2 × 10 mm quartz cuvette (Hellma, Plainview, NY), and measurements were blanked using the corresponding buffer solution. The data were exported and analyzed in Matlab to give the second-derivative spectrum calculated using a nine-point data filter and third-order Savitzky−Golay polynomial, as described elsewhere.[42] The wavelength shift of either the tyrosine or the tryptophan peak was determined from shifts in the local minima of the second-derivative spectra.

Ex-Situ Dynamic Light Scattering (DLS) with SEC. Dynamic light scattering was performed using a DAWN-HELEOS II with a QELS attachment (Wyatt). The autocorrelation function was collected as the aggregate and monomer peaks each eluted from the SEC column and subsequently flowed through the MALS instrument. The autocorrelation function data were exported and analyzed in Matlab with nonlinear regression to the cumulant equation described in eq 3 to give fitted parameters and their 95% confidence intervals[43,44]

$$g_2(\tau) = \alpha + \beta \exp(-2Q^2 D_0 \tau)\left(1 + \frac{\mu_2}{2!}\tau^2\right)^2 \tag{3}$$

where α is a constant for the short delay-time baseline, β is an instrument-specific constant, D_0 is the self-diffusion coefficient (at dilute protein concentrations), Q is the magnitude of the scattering vector defined in eq 4, n is the refractive index of solvent, λ is the laser wavelength (658.9 nm), θ is the scattering angle, τ is the decay time, and μ_2 is the second cumulant and related to the sample polydispersity index.

$$Q = \frac{4\pi n}{\lambda}\sin\left(\frac{\theta}{2}\right) \tag{4}$$

The average hydrodynamic radius, R_h, was calculated from fitted values for D_0 using the Stokes−Einstein relation (eq 5), where k_b is the Boltzmann constant, T is the absolute temperature, and η is the solvent viscosity.

$$R_h = \frac{k_b T}{6\pi\eta D_0} \tag{5}$$

In-Situ Dynamic Light Scattering with Raman Spectroscopy (DLS-Raman). Dynamic light scattering (DLS) with Raman spectroscopy experiments were performed on a Zetasizer Helix system (Malvern Instruments, Malvern, UK), which combines dynamic light scattering (DLS) with Raman spectroscopy. Raman scattering was excited by a 785 nm laser with approximately 280 mW power, while DLS was collected at the 173° backscattering angle from a 632 nm laser. For a typical experiment, ∼50 μL of sample was loaded into a titanium cuvette with a 120 μm quartz window (Malvern Instruments, Malvern, UK) and placed into a Peltier temperature-controlled sample compartment. Raman and DLS data were acquired in situ and semicontinuously, as the instrument allows one to alternate between Raman and DLS measurements while a sample is held continuously at a given temperature. To properly process the data, Raman spectra of corresponding buffer samples were acquired under identical conditions with the same experimental configuration. Unless otherwise noted, Raman spectra were collected with 20 coadditions of a 15 s exposure. Data were processed by first subtracting the background spectra and then normalizing by the intensity of the phenylalanine peak at ∼1003.5 cm^{-1}. Shifts in the Raman spectra were determined from a change in the center of mass (COM) of the second derivative as given by eq 6. $D(\nu)$ is the second-derivative

DOI: 10.1021/acs.jpcb.5b08748
J. Phys. Chem. B 2015, 119, 15150−15163

spectrum as a function of Raman shift, ν.[45] Detailed information regarding the Raman instrument, collection, and data analysis can be found elsewhere.[45−47]

$$COM = \frac{\int_{\nu_1}^{\nu_2} D(\nu)\nu \, d\nu}{\int_{\nu_1}^{\nu_2} D(\nu) d\nu} \quad (6)$$

Small Angle Neutron Scattering (SANS). Neutron scattering was performed on the 30 m NGB beamline at the NIST Center for Neutron Research (Gaithersburg, MD). For conditions at ambient temperatures, three configurations were used to collect the full Q range with 1, 5, and 13 m sample-to-detector distance (SDD) and a neutron wavelength of 6 Å. Among them, the detector was offset by 25 cm to allow a larger Q range at 5 m SDD. For in-situ conditions at elevated temperatures, scattering was collected using the 5 m SDD with 6 Å neutrons and 25 cm detector offset. Scattering data were corrected for detector background and sensitivity and the scattering contribution from empty cells. The protein scattering profiles were also reduced to the absolute intensity using the incident beam flux following the standard data reduction procedure with the Igor Pro NCNR software.[48] The Q dependence of the scattering is given by eq 7.[49] $I(Q)$ is the absolute intensity of scattered neutrons, $\Delta\rho$ is the neutron scattering length density difference between the protein and the buffer, V is the partial specific volume of the protein, $P(Q)$ is the particle form factor, $S(Q)$ is the structure factor, and B is a constant background.

$$I(Q) = \frac{c_2 M_w}{N_A}(\Delta\rho)^2(\widehat{V}_p)^2 P(Q)S(Q) + B \quad (7)$$

SANS was performed on unheated (monomer) AS-IgG1 at protein concentrations of 5, 10, and 30 mg/mL for each of the solution conditions. $S(Q)$ was calculated for 10 and 30 mg/mL solutions by assuming that $P(Q)$ is given by scattering intensity for 5 mg/mL. In a second set of experiments, SANS was performed on AS-IgG1 at each of the solution conditions while the protein was held at elevated temperature. For given solution conditions with and without 0.15 M sucrose, samples were inserted into a custom-built 10-cell sample changer pre-equilibrated to the desired temperature. The temperature was controlled with an external circulator of ethylene glycol flowing through the 10-cell sample chamber holder. A titanium cell with quartz windows was filled with water and inserted in the sample position adjacent to the protein sample. A calibrated thermocouple was inserted into the water cell, and temperature was logged during scattering experiments to ensure proper temperature control for the protein samples.

RESULTS

AS-IgG1 Aggregation Kinetics and Growth Mechanisms. Table 1 lists the solution conditions, aggregation mechanisms (determined below), and incubation temperature used to create aggregates.[29] In subsequent sections, the nomenclature for solution conditions follows the categorized growth mechanism in the far right column of Table 1 (e.g., ND, CP, CP/AP); the category CP/AP denotes that both CP and AP occur together on similar time scales, as noted previously for a number of proteins.[25,27,29,50] Aggregation was monitored at each solution condition and incubation temperature, in the presence and absence of 0.15 M sucrose. For a given solution condition (i.e., pD, NaCl concentration, and sucrose concentration), AS-IgG1 was heated at a selected elevated temperature, and vials were quenched on ice at different time points to effectively halt aggregation. Ex-situ characterization was performed with a combination of CD, second-deriviative UV absorption, and SEC-MALS with diluted quenched vials. In-situ DLS-Raman and SANS were used to monitor AS-IgG1 aggregation at the same temperature and using the same protein stock solutions as the above-mentioned quenched vials.

Table 1. Solution conditions, Aggregation Mechanisms, and Incubation Temperatures[a]

solution condition	aggregation mechanism	incubation temperature (°C)
pD 5.3, 10 mM acetate	nucleation dominated (ND)	69
pD 4.6, 100 mM NaCl, 10 mM acetate	chain polymerization (CP)	53
pD 5.1, 100 mM NaCl, 10 mM acetate	chain polymerization and association polymerization (CP/AP)	58

[a]All conditions were investigated in the presence and absence of 0.15 M sucrose.

The solution was diluted and SEC was performed to quantify the monomer fraction, which is defined as the fraction of the monomer peak area remaining for a heated sample relative to the monomer peak for unheated AS-IgG1. MALS inline with SEC was used to determine the molecular weight for eluting peaks. Incubation temperatures were selected to provide practically reasonable half-lives for monomer loss, based on short test experiments (not shown). Prior work showed that AS-IgG1 aggregates through the unfolding of the Fab domains for the range of solution conditions relevant here.[29] The particular solution conditions were selected to provide different aggregation mechanisms, based on earlier work with AS-IgG1 that mapped out different aggregation regimes based on pH and NaCl concentration on a 2 h monomer loss time scale at lower protein concentration (1 mg/mL).[29]

Figure 1A shows monomer fraction remaining, m, as a function of incubation time (t) for AS-IgG1 at pD 5.3 with 10 mM acetate (closed squares) and the addition of 0.15 M sucrose (open squares). The inset in Figure 1A shows $m(t)$ for AS-IgG1 pD 4.6 with 100 mM NaCl and 10 mM acetate (red circles) and pD 5.1, 100 mM NaCl, 10 mM acetate (black triangles). In all cases, open symbols correspond to conditions with 0.15 M sucrose also present and closed symbols to conditions without sucrose. AS-IgG1 aggregation growth mechanisms for these conditions are inferred from inspection of Figure 1B, which plots M_w^{tot}/M_0 as a function of $(1 - m)^2$. Symbol types correspond to the same conditions as Figure 1A. As shown previously,[25,27,29] plotting aggregation kinetics parametrically in this fashion allows one to determine the aggregation mechanism. Growth by monomer addition will result in a linear increase in M_w^{tot}/M_0 with $(1 - m)^2$. Growth via aggregate−aggregate coalescence will result in nonlinear increases in M_w^{tot}/M_0 that show upward curvature when plotted versus $(1 - m)^2$, as coalescence does not consume monomer and therefore does not alter m. Inspection of Figure 1B shows aggregation at pD 5.3, 10 mM acetate (blue squares) produces a mix of dimers and trimers and follows the ND mechanism (i.e., minimal growth). At pD 4.6, 100 mM NaCl, 10 mM (red circles), M_w^{tot} is linear with $(1 - m)^2$ and consistent with growth by monomer addition (i.e., the CP mechanism). AS-IgG1 at pD

DOI: 10.1021/acs.jpcb.5b08748
J. Phys. Chem. B 2015, 119, 15150−15163

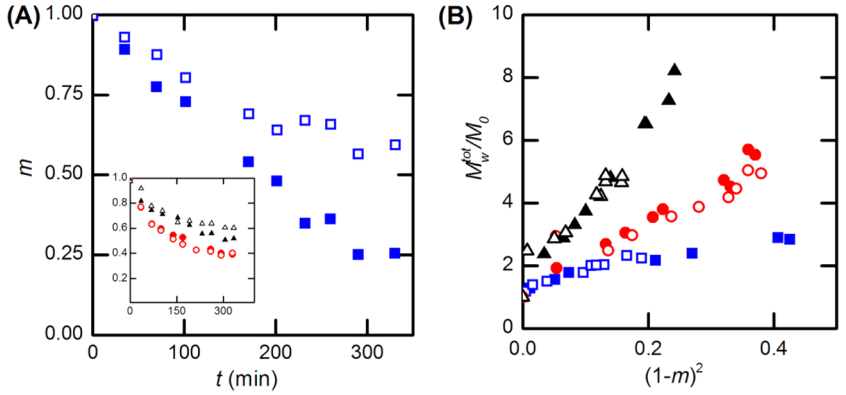

Figure 1. (A) Monomer fraction remaining as a function of time at elevated temperature for pD 5.3 heated at 69 °C (squares) and (inset) pD 5.1, 100 mM NaCl heated at 53 °C (circles) and pD 4.6, 100 mM NaCl heated at 58 °C(triangles). (B) M_w^{tot} vs $(1 - m)^2$ plot. In both panels, open symbols correspond to solutions with 0.15 M added sucrose.

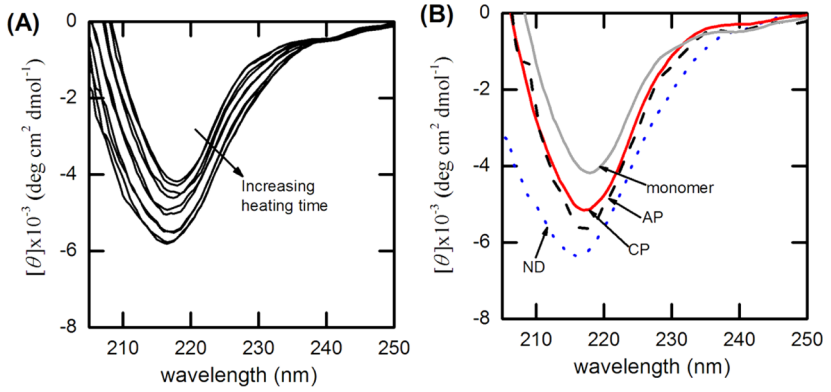

Figure 2. (A) Illustrative CD spectra over time AS-IgG1 pD 5.3 heated at 69 °C. Net aggregation contribution to the CD spectra for aggregate growth via ND (dotted blue), CP (dashed red), and AP (solid black) mechanism. An unheated monomer spectrum is shown as a gray solid line.

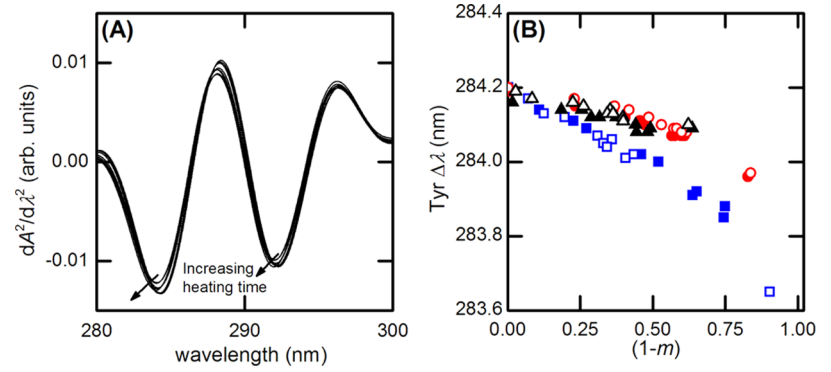

Figure 3. (A) Illustrative second-derivative UV−vis spectra over time for AS-IgG1 via ND growth. (B) Tyrosine center of mass shift as a function of monomer consumption $(1 - m)$. Symbols correspond to the same solution conditions as Figure 1.

5.1, 100 mM NaCl, 10 mM (black triangles) also follows CP growth and possibly AP growth at later stages as M_w^{tot}/M_0 appears to be curving slightly upward for larger values of $(1 - m)^2$. Comparison of Figure 1A and 1B shows that the addition of 0.15 M sucrose (open symbols) slows the overall aggregation rate(s) in some cases but has minimal or no change on the growth mechanism. For instance, for ND growth one observes slower monomer loss rates for sucrose compared to the buffer-only condition in Figure 1A, but sucrose and buffer-only conditions have identical M_w^{tot}/M_0 profiles in Figure 1B. Interestingly, sucrose does not dramatically alter monomer loss rates or the growth mechanism for the CP or CP/AP conditions.

AS-IgG1 Structural Changes during Aggregation. For the samples corresponding to Figure 1, AS-IgG1 aggregation was quenched (cold temperature) after a given incubation time at elevated temperature, and samples were diluted to low protein concentration to be within the instrument working range for structural characterization using circular dichroism and second-derivative UV absorption. Figure 2A illustrates circular dichroism spectra for the case of ND growth over time from Figure 1. Previous work with AS-IgG1[25] and other proteins[41] has illustrated that CD spectra obtained for such

DOI: 10.1021/acs.jpcb.5b08748
J. Phys. Chem. B 2015, 119, 15150−15163

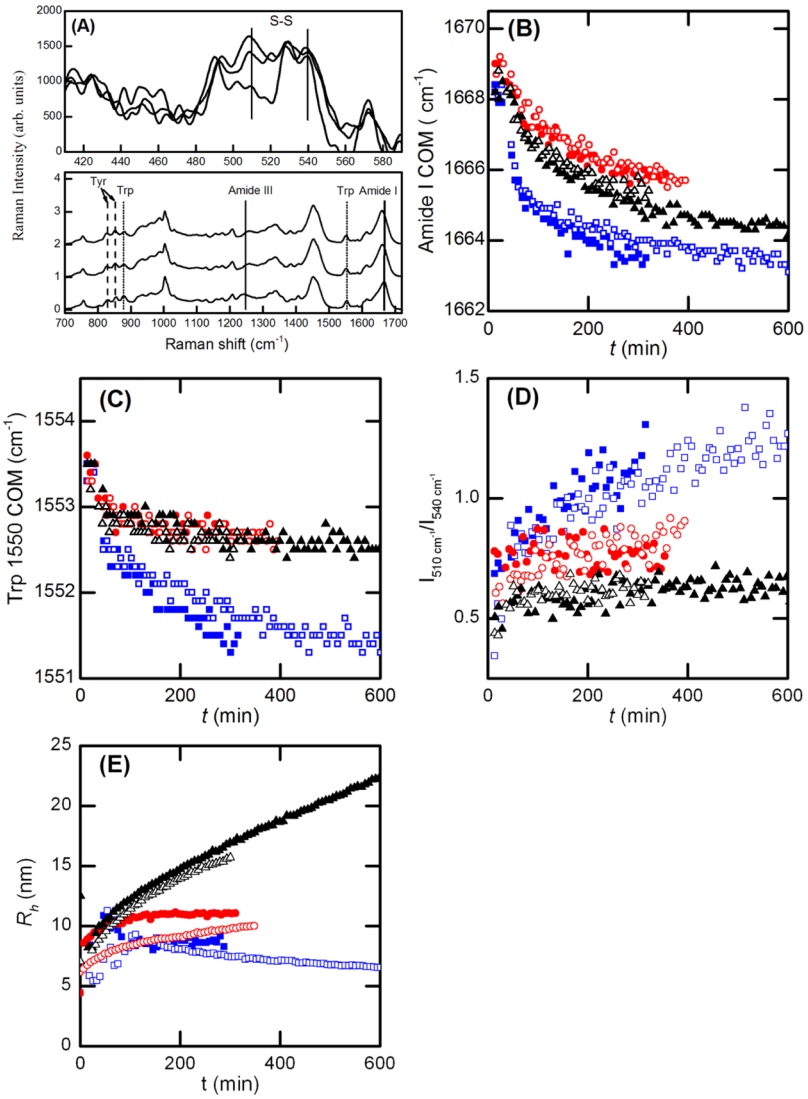

Figure 4. AS-IgG1 in-situ DLS-Raman (A). Illustrative Raman spectra for three time points at elevated temperature for IgG1 via ND growth. Raman markers plotted as a function of time for (B) amide I region and (C) Trp at 1550 cm^{-1}. (D) Ratio of Raman peak intensity at 510−540 cm^{-1} and (E) R_h over time. Symbols correspond to the same solution conditions as Figure 1.

quenched samples include contributions from the residual folded monomers and from the average over all aggregates in solution. As described in the Materials and Methods section, the CD spectra in Figure 2A were combined with the measured monomer fractions (cf. Figure 1A) and separately measured CD spectra for monomer (unheated) solutions to estimate the contribution to the CD spectra due to the aggregates via eqs 2a and 2b by subtracting the contribution from unaggregated monomer. This analysis assumes the monomer remaining maintains its native structure after incubations. The curves depicting $[\theta_{agg}]$ as a function of wavelength were found to be independent of incubation time for a given mechanism (see Supporting Information). This supports the "two-state" treatment of the CD data using eqs 2a and 2b and is consistent with monomer maintaining it is native structure and with prior treatments.[25,41] Figure 2B shows $[\theta_{agg}]$ versus wavelength for ND (blue dotted), CP (red solid), and CP/AP (black dashed) growth mechanisms. The CD spectrum for unheated AS-IgG1 monomer (solid gray line) is also shown. In Figure 2B, one observes distinguishable differences in the CD spectra when comparing the different growth mechanisms. This suggests the underlying aggregate structure may depend on the growth mechanism (see Discussion). All of the aggregate spectra are qualitatively consistent with increased beta-sheet content compared to the monomer structure, which is expected based on results for other aggregation-prone proteins.[51−53]

Figure 3A shows illustrative second-derivative UV absorption spectra for the conditions that show a ND aggregation mechanism from Figure 1. The minima at 284 and 292 nm correspond to the tyrosine (Tyr) and tryptophan (Trp) residues, respectively, and shift to lower wavelengths as aggregation proceeds. Prior work has shown that such peak shifts correspond to changes in $\pi-\pi$ interactions of the Tyr and Trp aromatic side chains, which are sensitive to the Trp and Tyr microenvironment and solvent accessibility.[54] Figure 3B quantifies how much the Tyr peak shifts for different AS-IgG1 growth mechanism as a function of the extent of monomer loss $(1 - m)$. The results are similar for the Trp peak shift (see Supporting Information). From Figure 3B, ND growth appears to have a much larger blue shift in the Tyr peak compared to CP or CP/AP growth. CP and CP/AP growth have linear decreases in Tyr peak shift, while ND growth has notable

DOI: 10.1021/acs.jpcb.5b08748
J. Phys. Chem. B 2015, 119, 15150−15163

downward curvature. The former is consistent with a relatively constant microenvironment during the aggregation process, while the latter suggests the aggregate Tyr microenvironment is changing as aggregation proceeds since the change in signal is not simply linear in the extent of mass converted from monomer to aggregate. Protein unfolding is expected to exhibit a blue shift as the protein unfolds and aromatic side chains become exposed.[55] However, conditions were not identified that allowed only unfolding to occur for AS-IgG1, which would have allowed a quantitative comparison between the changes in second-derivative UV spectra for aggregates and unfolded monomers. Interestingly, Tyr microenvironment(s) of the aggregate is(are) not affected by the presence of sucrose, as conditions with and without sucrose overlap in Figure 3B.

IgG Aggregation Monitored with in-Situ DLS-Raman. In-situ DLS-Raman measurements were performed at 30 mg/mL for each of the solution conditions illustrated in Figure 1. In what follows, the symbol shapes and colors correspond to the same conditions as in Figure 1. The bottom portion of Figure 4A illustrates typical Raman spectra for AS-IgG1. The bottom spectrum corresponds to initial, unheated sample, while the middle and top spectra correspond to the spectra at approximately 2 and 5 h at elevated temperature, respectively. The Raman spectra contain many different structural markers that may be monitored during aggregation; a few are indicated with vertical lines that are added in Figure 4A as guides to the eye. In particular, Tyr (dashed lines) and Trp (dotted lines) markers are sensitive to the microenvironment around the aromatic side chains, and amide I and amide III regions (solid lines) are pertinent to changes in the structure of the protein backbone (e.g., helix vs sheet structures). Additionally, the top half of Figure 4A depicts the Raman spectra for a subset of the range of wavenumbers (400−600 cm^{-1}), which contains information regarding the disulfide bonds.

Figure 4B plots the amide I center of mass (COM) as a function of time at elevated temperature for each condition from Figure 1. The amide I region shows a red shift as the protein aggregates and follows a roughly exponential decay vs time. To a first approximation, 80% of the amide I signal corresponds to the carbonyl vibration mode, 10% corresponds to N−H bond bending, and the remaining 10% corresponds to C−N bond stretching.[56] The amide I region provides information with respect to changes in secondary structure because the carbonyl and amide groups on the protein backbone participate in hydrogen bonding that stabilizes alpha helices, beta sheets, and/or beta barrels. Inspection of Figure 4B indicates that ND aggregation (squares) results in the largest change in the amide I region, followed by CP/AP (triangles) and then CP (circles). The symbols that correspond to sucrose (open symbols) and buffer-only (closed symbols) solution conditions overlap with each other for CP/AP and CP cases but not so for ND. This is consistent with the aggregation rates in Figure 1A, where sucrose slowed aggregation for the ND case but did not significantly slow aggregation for the other cases tested.

Typically, a blue shift in the amide I region is observed with protein unfolding or aggregation using FTIR or Raman.[56] However, in the present case, AS-IgG1 solutions were prepared in D_2O, and the protein backbone may exchange a hydrogen atom for that of deuterium as the protein unfolds and aggregates. The heavier D atoms are expected to slow the vibrational modes and lead to a red shift in the Raman amide I region, as has been observed previously.[57−59] The amide III region, which is predominantly N−H bending mode, showed significant changes, and these are attributed to H−D exchange on the protein backbone (see Supporting Information). However, it was not possible to deconvolute hydrogen−deuterium exchange from protein structural changes in the amide I region in this case. Detectable H−D exchange is expected to only occur for regions of the IgG1 that become exposed at elevated temperature, because all protein solutions were prepared and equilibrated in D_2O buffer for multiple days before incubation. The trends in the Raman shifts observed in the amide I region in Figure 4 are consistent with aggregation convoluted with H−D exchange. A comparative study with these spectroscopic techniques in H_2O was not performed and will be the subject of future work.

Raman spectra offer multiple markers to monitor aggregation that may or may not be convoluted by H−D exchange. The Tyr markers exhibited changes as AS-IgG1 was heated; however, the markers at 830 and ∼857 cm^{-1} are sensitive to the hydrogen bonding of the phenoxyl group in the Tyr side chain and may be convoluted with H−D exchange (see Supporting Information).[58] In contrast, Figure 4C shows how the Trp marker at 1550 cm^{-1} changes over time at elevated temperature. This peak arises from vibration modes of the aromatic side chain and the peptide-bond plane. It gives a relative measure of the protein tertiary structure and is not expected to be convoluted by H−D exchange. Inspection of Figure 4C shows a red shift for the Trp marker as the protein is heated and aggregates. Interestingly, the red shift is more pronounced for the ND case compared to CP/AP and CP cases. It is also notable that the CP and CP/AP cases have Raman shifts that are indistinguishable. Again, one observes that conditions with sucrose are similar to conditions with buffer only.

Raman spectroscopy also provides insights into the conformation of disulfide bonded side chains. Figure 4D shows the ratio of the Raman intensity at 510−540 cm^{-1}, which is sensitive to the conformation and packing density of disulfide bonds. Particularly, the disulfide region is sensitive to the gauche (G) and trans (T) conformers of the CCSSCC group.[56] The Raman intensity at 510 cm^{-1} is attributed to the S−S stretching of the GGG conformer, while the intensity at 540 cm^{-1} corresponds to the S−S stretching of the TGT conformer. Interestingly, as aggregation proceeds, the ND case has larger perturbation in this disulfide marker compared to CP or CP/AP cases.

In-situ DLS was performed along with Raman scattering for the samples and conditions in Figure 4A−C. Figure 4E plots the z-averaged apparent hydrodynamic radius as a function of time at elevated temperature, which was calculated from the diffusion coefficient using the Stokes−Einstein relation (cf. Materials and Methods). The increase in solution viscosity due to D_2O and sucrose at elevated temperature was accounted for in determining R_h.[60,61] The presence of aggregates may also increase viscosity, as has been shown previously, but such increases were not accounted for here and are expected to be relatively small contributions becuase aggregates did not grow as large as in previous studies.[62] Inspection of Figure 4E shows that the ND case produces aggregates that are relatively small, on average (i.e., less than ∼10 nm for the effective R_h), while the CP and CP/AP cases reach values of R_h near and well above 10 nm, respectively. These differences in R_h are qualitatively consistent with the sizes (molecular weight values) in Figure 1B. As DLS was collected in situ at 30 mg/mL, protein−protein interactions and hydrodynamic effects may convolute the z-

DOI: 10.1021/acs.jpcb.5b08748
J. Phys. Chem. B 2015, 119, 15150−15163

averaged diffusion coefficient and the corresponding apparent R_h values. This may be one possible explanation for why the apparent R_h decreases with increasing incubation time at later stages for the ND case.

Scaling of Aggregate M_w^{agg} and R_h. In SEC-MALS, samples are necessarily very dilute and the aggregate peak(s) are separated from the monomer. Therefore, the average aggregate molecular weight (M_w^{agg}) and hydrodynamic radius (R_h) determined using SEC-MALS do not have any contributions from the monomer and are not expected to be convoluted with protein−protein interactions. However, dilution may also result in the dissociation of reversible aggregates that are only observable at higher concentration and/or at elevated temperatures.[63] Figure 5 shows the scaling of M_w^{agg} and R_h, as this type of scaling plot gives a qualitative measure of aggregate morphology.[64,65] Each data point in Figure 5 corresponds to a slice of the aggregate peak eluting in SEC-MALS for a given sample condition, with samples quenched (see Materials and Methods) prior to injection for SEC. The symbols correspond to the same conditions as in Figures 1, 3B, and 4. Interestingly, all of the profiles follow a similar linear, almost overlapping, trend. This is reasonable given that the range of M_w^{agg} and R_h data for the ND case overlaps with that for the CP case but not the CP/AP case, while the CP data overlap with both ND with CP/AP cases. The solid lines in Figure 5 provide guides to the eye for slopes of 1, 2, and 3. Overall, the data show a linear slope with a value between 1 and 2. This is a similar average size-to-mass scaling as in previous work with this protein for lower protein concentrations and H_2O-based solution conditions, although aggregates did not reach sizes in the present case that were as large as in prior work.[29]

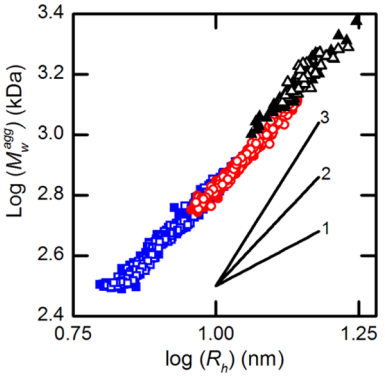

Figure 5. Scaling between M_w^{agg} and R_h. Symbols correspond to the same solution conditions as Figure 1. Black lines correspond to slopes of 1, 2, and 3.

IgG1 Monomer Structure Factor Using Small Angle Neutron Scattering (SANS). Small angle neutron scattering was performed on unheated AS-IgG1 solutions at concentrations of 5, 10, and 30 mg/mL for each condition. Figure 6A illustrates scattering intensity, $I(Q)$, after subtracting the background. As is common practice for protein solutions, the corresponding structure factor, $S(Q)$, was calculated by assuming the scattering profile for the lowest concentration (5 mg/mL) was dominated by the form factor because proteins are relatively weak scatters and $S(Q) \rightarrow 1$ at low protein concentrations.[12] Figure 6B shows $S(Q)$ for 10 and 30 mg/mL with buffer only and with the addition of 0.15 M sucrose for pD 5.3 (buffer only) conditions. $S(Q)$ is a measure of the net protein−protein interactions (PPI) in solution. Values less (greater) than 1 correspond to net repulsive (attractive) PPI. $S(Q)$ as Q approaches zero is related to the osmotic compressibility[49] and the Kirkwood−Buff integral for protein−protein interactions.[66] However, at Q values larger than ~0.03 A^{-1}, $S(Q)$ approaches a value of 1 and $I(Q)$ at that range of Q is dominanted by monomer or aggregate morphology. Figure 6B indicates net repulsive PPI at 10 and 30 mg/mL. On the basis of this analysis, the solution conditions at pD 5.3, 10 mM acetate have the strongest repulsive PPI, followed by pD 4.6 with 100 mM NaCl, 10 mM acetate and followed by pD 5.1, 100 mM NaCl in 10 mM acetate (see Supporting Information). Interestingly, the addition of sucrose does not affect the Q-dependent PPI in any of these cases. Prior work has shown that repulsive electrostatic PPI mediate IgG1 aggregation mechanisms at elevated temperature,[29] consistent with the observation above that sucrose does not alter the aggregation mechanisms.

In-Situ IgG Aggregation Using SANS. For each solution condition in Figure 1, protein aggregation was monitored in situ using SANS at elevated temperatures. Figure 7A illustrates the SANS $I(Q)$ profiles over time at elevated temperature for the CP case in buffer only (black curves) and with the addition of 0.15 M sucrose (blue curves). As aggregation occurs, the scattering intensity at low Q increases, indicating an increase in total weight-averaged molecular weight. The scattering at low to intermediate Q decreases with time, which is consistent with

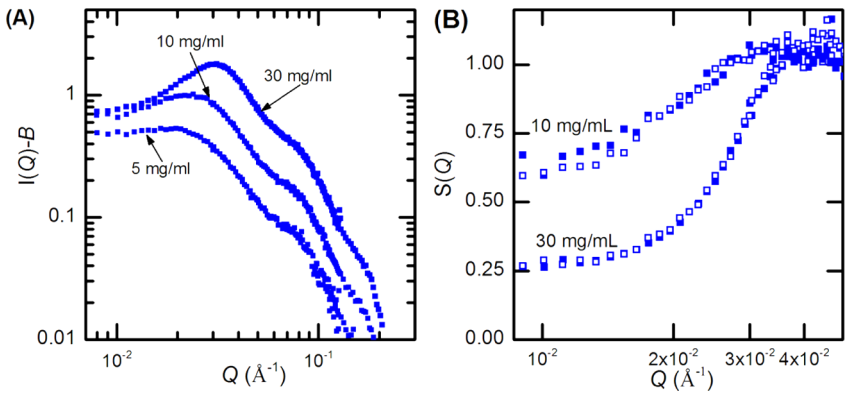

Figure 6. (A) SANS intensity as a function of Q for unheated (monomer) AS-IgG1 at pD 5.3 and protein concentration of 5, 10, and 30 mg/mL. (B) Structure factor as a function of Q. Closed symbols correspond to buffer only, and open symbols correspond to buffer with 0.15 M sucrose.

DOI: 10.1021/acs.jpcb.5b08748
J. Phys. Chem. B 2015, 119, 15150−15163

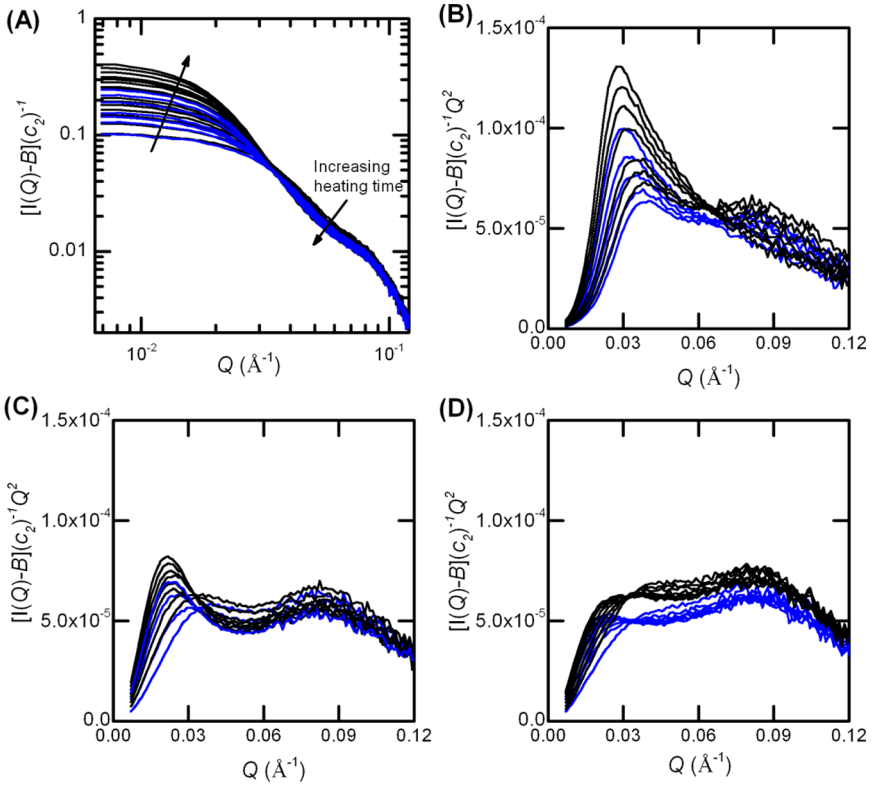

Figure 7. (A) AS-IgG1 in-situ SANS. (A) pD 4.6 with 100 mM NaCl and protein concentration of 30 mg/mL heated at 53 °C. Kratky plots for AS-IgG1 over time at elevated temperature. (B) pD 5.3 heated at 69 °C; (C) pD 4.6 with 100 mM NaCl heated at 53 °C; (D) pD 5.1 with 100 mM NaCl heated at 58 °C. Black curves correspond to buffer only, while blue curves are for 0.15 M sucrose.

change of monomer conformation as it unfolds and aggregates. SANS was performed in situ at elevated temperatures and aggregation occurs over multiple hours. It is expected that the concentration of unfolded "reactive" monomer will be pre-equilibrated and be only a small fraction of the total monomer population (0.1−10%).[26] For the buffer-only conditions in Figure 7A, aggregates grew to larger sizes (for a given time point) compared to the same condition with added sucrose, which is consistent with Figure 1B because aggregation rates were slower in the presence of sucrose.

In-situ SANS profiles were analyzed using so-called Kratky plots, which show $I(Q)Q^2$ plotted against Q.[49] Traditionally, Kratky plots are used to investigate polymer conformational changes. For semiflexible polymers, the profile in a Kratky plot plateaus at high Q values, while for polymers in a globular conformation the profiles will reach a maximum at intermediate Q values and then decrease toward a value of zero at high Q values. Additionally, normalizing the scattering intensity to $I(0)$ and normalizing Q to the radius of gyration or the volume of correlation provides a useful tool to compare the conformation of various polymers or proteins with different M_w or R_g (see Supporting Information).[67]

For the ND case, a significant structure factor contribution was observed and it was not possible to determine reliable $I(0)$ or R_g from a traditional Guinier analysis (not shown). Figure 7B shows Kratky plots for ND growth. One observes from Figure 7B that as aggregation proceeds, the peak at higher Q values decreases, suggesting monomer consumption leads to a loss in scattering in this high-Q region. Additionally, the peak at lower Q values increases over time at elevated temperatures. However, as observed in Figure 6, there is a significant influence of the structure factor at Q values less than 0.03 A^{-1}, and therefore, it is difficult to separate changes in the SANS profiles at these larger length scales where long-ranged interparticle electrostatic interactions convolute with aggregate morphology. As mentioned above, for Q values greater than about 0.03 A^{-1} the value for the structure factor is essentially 1 and changes in the scattering intensity can be attributed to changes in the IgG1 conformation.[49]

Figure 7C and 7D shows the Kratky plots for CP (Figure 7C) and CP/AP (Figure 7D) cases. Kratky plots allow one to compare changes in average aggregate morphology for aggregates across various sizes and for a wider range of the extent of monomer loss. Inspection of Figure 7C and 7D shows that as aggregation proceeds, the first peak (at low values of Q) increases slightly, while the second peak (higher Q values) tends to decrease. The first peak is indicative of the average mass and radius of the overall particle size distribution, while the secondary peak is related to average mass and size at much smaller length scales, such as the internal structure of the monomeric protein.

The profiles in Figure 7B have a peak at low Q values, which is indicative of the average particle mass and size. In the case of a fully unfolded protein that behaves similarly to an extended polymer, the Kratky plot is expected to increase at low Q values and reach a plateau.[67] In contrast, the CP/AP case in Figure 7D does not have as well defined peak at low Q, possibly indicating increased flexibility of extended structures. Aggregates in the CP/AP case have larger average M_w^{tot} and R_g values compared to ND and CP cases. Overall, the time-dependent profiles in Figure 7B and 7D are qualitatively different for each of the aggregation mechanisms tested here. Interestingly, the addition of sucrose slows aggregation, but the profiles with and without sucrose are similar, again suggesting that sucrose does not play

DOI: 10.1021/acs.jpcb.5b08748
J. Phys. Chem. B 2015, 119, 15150−15163

a role in the underling growth process. See the Supporting Information for more details regarding Kratky plots and normalizing the scattering profiles to $I(Q = 0)$ and R_g.

DISCUSSION

In the present context, the aggregation mechanisms are categorized by how M_w^{tot}/M_0 scales with the extent of monomer loss, and this also determines how large aggregates will grow via one or more mechanisms (e.g., CP and AP). Prior work has shown that altering the solution pH and salt concentration mediates electrostatic protein−protein interactions and ultimately the mechanisms of aggregate growth or lack thereof. Results at low concentration also indicated that the protein secondary structure within aggregates was less (more) perturbed when aggregates formed at solution conditions that correspond to weaker (stronger) intermolecular repulsions and higher (lower) T_m values.[25] In the present work, the solution conditions (i.e., pD and NaCl concentration) were chosen to align with different aggregate growth mechanisms found at low protein concentration (1 mg/ml) in H_2O-based solutions. The present work focuses on the aggregate structure and morphology and possible connections with aggregation mechanisms at higher protein concentrations as well as how these may be affected by the change from H_2O to D_2O that was necessitated by using SANS.

Structural Changes during Aggregation. The CD, second-derivative UV, and Raman spectra all show that the underlying protein structure within aggregates is most perturbed, compared to unheated monomer structures, for aggregates created under the ND condition. The second-derivative UV results not only showed larger structural changes for the ND condition but also exhibited a nonlinear decrease in Tyr peak position with monomer consumption. This suggests the protein structure within aggregates for the ND case is changing as aggregates grow from dimer to trimer. CP and CP/AP conditions in this work and prior work with a globular protein have shown that shifts in CD and intrinsic fluorescence spectra were linear with respect to the loss of monomer. That was interpreted as an indication that each monomer that was incorporated into an aggregate, no matter the size of the aggregate, underwent a similar structural change as part of that process; aggregate−aggregate coalescence did not result in significant changes in those spectroscopic signals because the constituent monomers had already undergone the structural change(s) needed for them to incorporate into the aggregates.

ND conditions result in little or no aggregate growth, and there are much larger concentrations of dimers and small oligomer than for the CP and AP cases. It is speculated that dimer formation may involve a larger structural change for a constituent monomer compared to when large aggregates incorporate monomers as they grow via monomer addition via CP. Alternatively, it may simply be that the solution conditions that promote ND behavior require such repulsive interprotein interactions (e.g., strong electrostatic repulsions) that this also promotes larger intraprotein repulsions that lead to larger structural perturbations upon unfolding and aggregation. The observations here cannot reconcile which of these interpretations should be afforded a "causal" relationship to the observed results, but they do support a correlation between ND behavior and large structural perturbations that was noted previously at lower protein concentrations for two different MAbs.[24,25]

Raman scattering provided an orthogonal technique to probe aggregate structure. Consistent with CD and second-derivative UV results, ND growth resulted in larger structural changes in the disulfide-bonded side chains and Trp markers, which were not convoluted with H−D exchange. Additionally, disulfide bonds were much more perturbed for ND growth compared to the other mechanisms, suggesting larger tertiary structural changes may occur while ND growth proceeds. While beyond the scope of this work, one may hypothesize that aggregates created via CP and CP/AP growth, which have less structural changes and grow to larger sizes, may have increased immunogenicity concerns because they more closely resemble the native IgG structure.[4,9]

Aggregate Morphology from Kratky Plots. The scaling of aggregate M_w^{tot} and R_h in Figure 5 shows a linear relationship between aggregate mass and size. It is difficult to discern if dimer or trimer subpopulations under AP conditions produce aggregates with a similar mass-to-size scaling for ND conditions because the scattering under AP conditions is biased toward the much larger particles in solution. However, SANS provides a more detailed technique to monitor aggregate morphology. SANS profiles at higher Q values can be attributed to IgG monomer contributions, while the low-Q scattering is predominantly attributed to the aggregates. The SANS Kratky plot profiles allow one to monitor the evolution of the qualitative aggregate morphology. Interestingly, each of the growth mechanisms produces a discernably different qualitative SANS profile.

As observed previously for this IgG1 and other proteins, the solution conditions (i.e., pH, NaCl, buffer) mediate the aggregation mechanism. As mentioned above, the addition of sucrose does not affect the aggregation mechanism in terms of the M_w^{tot} profiles in Figure 1B, and Kratky plots in Figure 7B and 7D appear identical for a given mechanism in buffer-only conditions or with sucrose present. Similarly, the spectroscopic profiles over time, or compared to the amount of monomer consumed, were unaffected by the presence of sucrose. Taken together, the results indicate that sucrose acts to slow the process of aggregation in some cases but does not change the underlying mechanism(s) of aggregation. Presumably, sucrose slows aggregation by increasing the free energy of unfolding for the structural changes within the monomer that are precursors to nucleation, and this is consistent with previous reports[35,68] and with the observation that sucrose had the greatest effect on AS-IgG1 aggregation rates for ND conditions.

The SANS data and Kratky plot analysis provide insight into the compactness or flexibility of aggregates that is not afforded by the other techniques. Prior work in dilute protein concentrations, where negligible structure factor contributions were observed, showed ND conditions produce a relatively compact morphology.[29] While in the present case the Kratky plot for ND conditions (Figure 7B) is convoluted with structure factor effects, results are consistent with a compact morphology. Additionally, the Kratky plot for CP conditions initially shows a well-defined peak at low Q, suggesting the average mass and size have a relatively compact morphology. However, as aggregation proceeds, the low-Q peak broadens, suggesting the average aggregate flexibility increases with growth. Dimers and trimers may be expected to both have a compact morphology, but larger sized aggregates may have increased flexibility, and this would influence the SANS signal as aggregates grow. The Kratky plot for CP/AP growth does not have a well-defined peak at lower Q values, suggesting that process produces a more flexible aggregate morphology. One can speculate that this would be consistent with low fractal-

DOI: 10.1021/acs.jpcb.5b08748
J. Phys. Chem. B 2015, 119, 15150−15163

dimension aggregates that result from association of multiple aggregates during the AP process. From the mass to size scaling in Figure 5 one observes the slope or fractal dimension has a value just less than 2, which is similar to values for polymer-chain- (∼1.7) or diffusion-limited-aggregate morphology (∼1.86).[69] This fractal dimension is consistent with the flexibility of CP/AP morphology observed in Kratky plots.

The Kratky plots also illustrate the secondary peak in the SANS profile located at intermediate Q values that has been previously attributed to the flexibility of the IgG1 hinge region.[70] As aggregation proceeds and monomer is consumed, this intermediate-Q peak decreases, which may simply be indicative of the loss of monomer, given that the spectroscopic techniques generally show that the secondary and tertiary structure of protein chains in the aggregated state(s) are significantly different from that in the monomer state. The Kratky plot analysis also shows a decrease in the secondary peak at higher Q values, which is especially pronounced for ND conditions. This suggests that proteins lose much of their native structure as they incorporated into aggregates, consistent with the spectroscopic results for ND behavior discussed above. Overall, SANS provides a complementary tool to investigate aggregate morphology even at relatively high protein concentrations, and the analysis above illustrates an established means to interpret the results without the need to fit assumed models for structure factor or form factor.

Sucrose Affects Rates but Not Qualitative Features of Aggregation. Average aggregate structure and morphology were monitored as aggregation proceeded, with and without the addition of 0.15 M sucrose, for each of the solution conditions that gave rise to different mechanisms. As observed in Figure 1, the addition of sucrose tends to decrease the rate of aggregation rather than alter the qualitative growth mechanism/behavior. Additionally, sucrose markedly affects the rates in ND conditions but minimally affects rates for the CP or AP conditions. The CD, second-derivative UV absorption, and Raman spectra also indicate that sucrose has little effect on aggregation rates for CP or AP conditions here. Perhaps surprisingly, sucrose did not change the protein−protein interactions determined from SANS (i.e., $S(Q)$). Sucrose did alter how large aggregates grew, but normalizing the SANS profiles by size and mass revealed each growth mechanism overlaps with and without sucrose, indicating that this again is simply a question of the net rate of aggregation. This suggests that the sucrose does not alter the aggregate growth process or mechanism. Rather, it only decreases the rate of aggregation, consistent with its presumed role in decreasing the amount of unfolded monomer present in solution, as noted above and elsewhere.[71]

Sucrose and other saccharides are often added to protein solution as stabilizers. Sucrose is thought to be preferentially excluded from the protein surface as observed previously.[72,73] The preferential exclusion mechanism is expected to have a more pronounced effect on the unfolded state compared to that of the native state and therefore increase the free energy of unfolding.[74] As a result, the concentration of unfolded "reactive" monomers will decrease in the presence of sucrose, which will decrease the aggregation rate.[35] Additionally, if a mechanism is dominated by nucleation, such as the ND mechanism, one should observe a larger dependence on the monomer loss rate when one adds sucrose.[35] In contrast, if nucleation is dramatically slower than growth, such as the CP and AP mechanism, sucrose will have less of an effect on monomer loss rates. However, available models would predict that the rate of monomer loss would still be affected appreciably by the addition of sucrose. As such, the relatively small effect of sucrose on AS-IgG1 aggregation rates for CP and AP/CP conditions merits additional consideration and will be the focus of future work.

CONCLUSION

The aggregate structure and morphology were monitored for ND, CP, and CP/AP aggregation mechanisms for AS-IgG1 with and without sucrose present at typical formulation conditions (5 w/w %). Sucrose did not affect the aggregation mechanism(s) or the resulting aggregate structure or morphology. Sucrose decreased monomer loss rates, which was most pronounced for the nucleation-dominated mechanism. Protein structural characterization with CD, Raman, and second-derivative UV suggests aggregates via ND mechanism result in significantly larger structural perturbation compared to other growth mechanisms. In-situ DLS-Raman provided additional structural characterization that included local Tyr and Trp enviroments, disulfide bonding, and amide I and III markers along with the z-averaged R_h. SANS Kratky plots provided a tool to monitor aggregate morphology and monomer loss. Each growth mechanism showed a unique evolution of aggregate morphology with time in SANS, which complemented the structural changes detected with the other techniques. In general, aggregates that grew larger tended to exhibit increased flexibility. Overall, the results provide a comparison of aggregate structure and morphology using various orthogonal techniques for aggregates created via ND, CP, and AP growth mechanisms and suggest that solution conditions that promote only small aggregates may also promote aggregates composed of monomers that are more structurally perturbed than conditions that promote larger aggregates.

ASSOCIATED CONTENT

Supporting Information

The Supporting Information is available free of charge on the ACS Publications website at DOI: 10.1021/acs.jpcb.5b08748.

Additional details regarding net aggregate contribution to far-UV CD spectra, Trp peak shifts of the second-derivative UV, additional Raman markers, and SANS structure factor for AS-IgG1 at elevated protein concentration, and SANS normalized Kratky plots (PDF)

AUTHOR INFORMATION

Corresponding Author

*Phone: (1) 302-831-0838. Fax: (1) 302-831-1048. E-mail: cjr@udel.edu.

Present Address

‖B.A.K.: Just Biotherapeutics, Seattle, Washington 98109, United States.

Notes

The authors declare no competing financial interest.

ACKNOWLEDGMENTS

G.V.B. and C.J.R. gratefully acknowledge support from Amgen, the National Institute of Standards and Technology (NIST 70NANB12H239), and the National Science Foundation

DOI: 10.1021/acs.jpcb.5b08748
J. Phys. Chem. B 2015, 119, 15150−15163

(CBET 0931173). This work used the NGB (30m SANS) instrument at the National Institute of Standards and Technology Center for Neutron Research (NCNR, Gaithersburg, MD). Certain commercial equipment, instruments, or materials (or suppliers, or software) are identified in this paper to foster understanding. Such identification does not imply recommendation or endorsement by the National Institute of Standards and Technology nor does it imply that the materials or equipment identified are necessarily the best available for the purpose.

REFERENCES

(1) Ecker, D. M.; Jones, S. D.; Levine, H. L. The Therapeutic Monoclonal Antibody Market. *mAbs* **2015**, *7*, 9−14.
(2) Baker, M. P.; Reynolds, H. M.; Lumicisi, B.; Bryson, C. J. Immunogenicity of Protein Therapeutics. *Self Nonself* **2010**, *1*, 314−322.
(3) Ratanji, K. D.; Derrick, J. P.; Dearman, R. J.; Kimber, I. Immunogenicity of Therapeutic Proteins: Influence of Aggregation. *J. Immunotoxicol.* **2014**, *11*, 99−109.
(4) Wang, W.; Singh, S. K.; Li, N.; Toler, M. R.; King, K. R.; Nema, S. Immunogenicity of Protein aggregates—Concerns and Realities. *Int. J. Pharm.* **2012**, *431*, 1−11.
(5) Wang, W.; Roberts, C. J. *Aggregation of Therapeutic Proteins*; John Wiley & Sons: New York, 2010.
(6) Liu, L. Antibody Glycosylation and Its Impact on the Pharmacokinetics and Pharmacodynamics of Monoclonal Antibodies and Fc-Fusion Proteins. *J. Pharm. Sci.* **2015**, *104*, 1866−1884.
(7) Gerhardt, A.; Bonam, K.; Bee, J. S.; Carpenter, J. F.; Randolph, T. W. Ionic Strength Affects Tertiary Structure and Aggregation Propensity of a Monoclonal Antibody Adsorbed to Silicone Oil-Water Interfaces. *J. Pharm. Sci.* **2013**, *102*, 429−440.
(8) Fradkin, A. H.; Carpenter, J. F.; Randolph, T. W. Glass Particles as an Adjuvant: A Model for Adverse Immunogenicity of Therapeutic Proteins. *J. Pharm. Sci.* **2011**, *100*, 4953−4964.
(9) Kumar, S.; Mitchell, M. A.; Rup, B.; Singh, S. K. Relationship between Potential Aggregation-Prone Regions and HLA-DR-Binding T-Cell Immune Epitopes: Implications for Rational Design of Novel and Follow-on Therapeutic Antibodies. *J. Pharm. Sci.* **2012**, *101*, 2686−2701.
(10) Shire, S. J.; Shahrokh, Z.; Liu, J. Challenges in the Development of High Protein Concentration Formulations. *J. Pharm. Sci.* **2004**, *93*, 1390−1402.
(11) Lilyestrom, W. G.; Yadav, S.; Shire, S. J.; Scherer, T. M. Monoclonal Antibody Self-Association, Cluster Formation, and Rheology at High Concentrations. *J. Phys. Chem. B* **2013**, *117*, 6373−6384.
(12) Yearley, E. J.; Zarraga, I. E.; Shire, S. J.; Scherer, T. M.; Gokarn, Y.; Wagner, N. J.; Liu, Y. Small-Angle Neutron Scattering Characterization of Monoclonal Antibody Conformations and Interactions at High Concentrations. *Biophys. J.* **2013**, *105*, 720−731.
(13) Shire, S. J.; Shahrokh, Z.; Liu, J. Challenges in the Development of High Protein Concentration Formulations. *J. Pharm. Sci.* **2004**, *93*, 1390−1402.
(14) Sahin, E.; Roberts, C. J. Size-Exclusion Chromatography with Multi-Angle Light Scattering for Elucidating Protein Aggregation Mechanisms. *Methods Mol. Biol.* **2012**, *899*, 403−423.
(15) Carpenter, J. F.; Randolph, T. W.; Jiskoot, W.; Crommelin, D. J. A.; Middaugh, C. R.; Winter, G. Potential Inaccurate Quantitation and Sizing of Protein Aggregates by Size Exclusion Chromatography: Essential Need to Use Orthogonal Methods to Assure the Quality of Therapeutic Protein Products. *J. Pharm. Sci.* **2010**, *99*, 2200−2208.
(16) Kalonia, C.; Kumru, O. S.; Prajapati, I.; Mathaes, R.; Engert, J.; Zhou, S.; Middaugh, C. R.; Volkin, D. B. Calculating the Mass of Subvisible Protein Particles with Improved Accuracy Using Microflow Imaging Data. *J. Pharm. Sci.* **2015**, *104*, 536−547.
(17) Wuchner, K.; Büchler, J.; Spycher, R.; Dalmonte, P.; Volkin, D. B. Development of a Microflow Digital Imaging Assay to Characterize Protein Particulates during Storage of a High Concentration IgG1 Monoclonal Antibody Formulation. *J. Pharm. Sci.* **2010**, *99*, 3343−3361.
(18) Filipe, V.; Hawe, A.; Jiskoot, W. Critical Evaluation of Nanoparticle Tracking Analysis (NTA) by NanoSight for the Measurement of Nanoparticles and Protein Aggregates. *Pharm. Res.* **2010**, *27*, 796−810.
(19) Vasudev, R.; Mathew, S.; Afonina, N. Characterization of Submicron (0.1−1 μm) Particles in Therapeutic Proteins by Nanoparticle Tracking Analysis. *J. Pharm. Sci.* **2015**, *104*, 1622−1631.
(20) Rayner, L. E.; Hui, G. K.; Gor, J.; Heenan, R. K.; Dalby, P. A.; Perkins, S. J. The Fab Conformations in the Solution Structure of Human Immunoglobulin G4 (IgG4) Restrict Access to Its Fc Region: Implications for Functional Activity. *J. Biol. Chem.* **2014**, *289*, 20740−20756.
(21) Amin, S.; Barnett, G. V.; Pathak, J. A.; Roberts, C. J.; Sarangapani, P. S. Protein Aggregation, Particle Formation, Characterization & Rheology. *Curr. Opin. Colloid Interface Sci.* **2014**, *19*, 438−449.
(22) Menzen, T.; Friess, W. High-Throughput Melting-Temperature Analysis of a Monoclonal Antibody by Differential Scanning Fluorimetry in the Presence of Surfactants. *J. Pharm. Sci.* **2013**, *102*, 415−428.
(23) Zhang, A.; Jordan, J. L.; Ivanova, M. I.; Weiss, W. F.; Roberts, C. J.; Fernandez, E. J. Molecular Level Insights into Thermally Induced α-Chymotrypsinogen A Amyloid Aggregation Mechanism and Semi-flexible Protofibril Morphology. *Biochemistry* **2010**, *49*, 10553−10564.
(24) Brummitt, R. K.; Nesta, D. P.; Chang, L.; Chase, S. F.; Laue, T. M.; Roberts, C. J. Nonnative Aggregation of an IgG1 Antibody in Acidic Conditions: Part 1. Unfolding, Colloidal Interactions, and Formation of High-Molecular-Weight Aggregates. *J. Pharm. Sci.* **2011**, *100*, 2087−2103.
(25) Kim, N.; Remmele, R. L.; Liu, D.; Razinkov, V. I.; Fernandez, E. J.; Roberts, C. J. Aggregation of Anti-Streptavidin Immunoglobulin gamma-1 Involves Fab Unfolding and Competing Growth Pathways Mediated by pH and Salt Concentration. *Biophys. Chem.* **2013**, *172*, 26−36.
(26) Wu, H.; Kroe-Barrett, R.; Singh, S.; Robinson, A. S.; Roberts, C. J. Competing Aggregation Pathways for Monoclonal Antibodies. *FEBS Lett.* **2014**, *588*, 936−941.
(27) Brummitt, R. K.; Nesta, D. P.; Chang, L.; Kroetsch, A. M.; Roberts, C. J. Nonnative Aggregation of an IgG1 Antibody in Acidic Conditions, Part 2: Nucleation and Growth Kinetics with Competing Growth Mechanisms. *J. Pharm. Sci.* **2011**, *100*, 2104−2119.
(28) Cohen, S. I. A.; Vendruscolo, M.; Dobson, C. M.; Knowles, T. P. J. From Macroscopic Measurements to Microscopic Mechanisms of Protein Aggregation. *J. Mol. Biol.* **2012**, *421*, 160−171.
(29) Barnett, G. V.; Razinkov, V. I.; Kerwin, B. A.; Laue, T. M.; Woodka, A. H.; Butler, P. D.; Perevozchikova, T.; Roberts, C. J. Specific-Ion Effects on the Aggregation Mechanisms and Protein−Protein Interactions for Anti-Streptavidin Immunoglobulin Gamma-1. *J. Phys. Chem. B* **2015**, *119*, 5793−5804.
(30) Paul, R.; Graff-Meyer, A.; Stahlberg, H.; Lauer, M. E.; Rufer, A. C.; Beck, H.; Briguet, A.; Schnaible, V.; Buckel, T.; Boeckle, S. Structure and Function of Purified Monoclonal Antibody Dimers Induced by Different Stress Conditions. *Pharm. Res.* **2012**, *29*, 2047−2059.
(31) Bessa, J.; Boeckle, S.; Beck, H.; Buckel, T.; Schlicht, S.; Ebeling, M.; Kiialainen, A.; Koulov, A.; Boll, B.; Weiser, T.; et al. The Immunogenicity of Antibody Aggregates in a Novel Transgenic Mouse Model. *Pharm. Res.* **2015**, *32*, 2344−2359.
(32) Hawe, A.; Kasper, J. C.; Friess, W.; Jiskoot, W. Structural Properties of Monoclonal Antibody Aggregates Induced by Freeze−thawing and Thermal Stress. *Eur. J. Pharm. Sci.* **2009**, *38*, 79−87.
(33) Hawe, A.; Wiggenhorn, M.; van de Weert, M.; Garbe, J. H. O.; Mahler, H.; Jiskoot, W. Forced Degradation of Therapeutic Proteins. *J. Pharm. Sci.* **2012**, *101*, 895−913.

DOI: 10.1021/acs.jpcb.5b08748
J. Phys. Chem. B 2015, 119, 15150−15163

(34) Joubert, M. K.; Luo, Q.; Nashed-Samuel, Y.; Wypych, J.; Narhi, L. O. Classification and Characterization of Therapeutic Antibody Aggregates. *J. Biol. Chem.* **2011**, *286*, 25118−25133.
(35) Banks, D. D.; Latypov, R. F.; Ketchem, R. R.; Woodard, J.; Scavezze, J. L.; Siska, C. C.; Razinkov, V. I. Native-State Solubility and Transfer Free Energy as Predictive Tools for Selecting Excipients to Include in Protein Formulation Development Studies. *J. Pharm. Sci.* **2012**, *101*, 2720−2732.
(36) Rajanikanth, V.; Srivastava, S. S.; Singh, A. K.; Rajyalakshmi, M.; Chandra, K.; Aravind, P.; Sankaranarayanan, R.; Sharma, Y. Aggregation-Prone Near-Native Intermediate Formation during Unfolding of a Structurally Similar Nonlenticular $\beta\gamma$-Crystallin Domain. *Biochemistry* **2012**, *51*, 8502−8513.
(37) Bemporad, F.; De Simone, A.; Chiti, F.; Dobson, C. M. Characterizing Intermolecular Interactions That Initiate Native-Like Protein Aggregation. *Biophys. J.* **2012**, *102*, 2595−2604.
(38) Covington, A. K.; Paabo, M.; Robinson, R. A.; Bates, R. G. Use of the Glass Electrode in Deuterium Oxide and the Relation between the Standardized pD (paD) Scale and the Operational pH in Heavy Water. *Anal. Chem.* **1968**, *40*, 700−706.
(39) Andrews, J. M.; Roberts, C. J. Non-Native Aggregation of α-Chymotrypsinogen Occurs through Nucleation and Growth with Competing Nucleus Sizes and Negative Activation Energies †. *Biochemistry* **2007**, *46*, 7558−7571.
(40) Kelly, S. M.; Jess, T. J.; Price, N. C. How to Study Proteins by Circular Dichroism. *Biochim. Biophys. Acta, Proteins Proteomics* **2005**, *1751*, 119−139.
(41) Li, Y.; Ogunnaike, B. A.; Roberts, C. J. Multi-Variate Approach to Global Protein Aggregation Behavior and Kinetics: Effects of pH, NaCl, and Temperature for Alpha-Chymotrypsinogen A. *J. Pharm. Sci.* **2010**, *99*, 645−662.
(42) Ultraviolet Absorption Spectroscopy of Peptides-Springer. In *Methods in Molecular Biology*; Nixon, A. E., Ed.; Humana Press, 2014.
(43) Frisken, B. J. Revisiting the Method of Cumulants for the Analysis of Dynamic Light-Scattering Data. *Appl. Opt.* **2001**, *40*, 4087−4091.
(44) Koppel, D. E. Analysis of Macromolecular Polydispersity in Intensity Correlation Spectroscopy: The Method of Cumulants. *J. Chem. Phys.* **1972**, *57*, 4814−4820.
(45) Lewis, E. N.; Qi, W.; Kidder, L. H.; Amin, S.; Kenyon, S. M.; Blake, S. Combined Dynamic Light Scattering and Raman Spectroscopy Approach for Characterizing the Aggregation of Therapeutic Proteins. *Molecules* **2014**, *19*, 20888−20905.
(46) Zhou, C.; Qi, W.; Neil Lewis, E.; Carpenter, J. F. Concomitant Raman Spectroscopy and Dynamic Light Scattering for Characterization of Therapeutic Proteins at High Concentrations. *Anal. Biochem.* **2015**, *472*, 7−20.
(47) Amin, S.; Blake, S.; Kenyon, S. M.; Kennel, R. C.; Lewis, E. N. A Novel Combination of DLS-Optical Microrheology and Low Frequency Raman Spectroscopy to Reveal Underlying Biopolymer Self-Assembly and Gelation Mechanisms. *J. Chem. Phys.* **2014**, *141*, 234201.
(48) Kline, S. R. Reduction and Analysis of SANS and USANS Data Using IGOR Pro. *J. Appl. Crystallogr.* **2006**, *39*, 895−900.
(49) In *Neutron, X-Rays and Light. Scattering Methods Applied to Soft Condensed Matter*, 1st ed.; Zemb, T., Lindner, P., Eds.; North Holland: Amsterdam, Boston, 2002.
(50) Li, Y.; Roberts, C. J. Lumry−Eyring Nucleated-Polymerization Model of Protein Aggregation Kinetics. 2. Competing Growth via Condensation and Chain Polymerization. *J. Phys. Chem. B* **2009**, *113*, 7020−7032.
(51) Weiss, W. F.; Hodgdon, T. K.; Kaler, E. W.; Lenhoff, A. M.; Roberts, C. J. Nonnative Protein Polymers: Structure, Morphology, and Relation to Nucleation and Growth. *Biophys. J.* **2007**, *93*, 4392−4403.
(52) Brogan, A. P. S.; Sharma, K. P.; Perriman, A. W.; Mann, S. Isolation of a Highly Reactive β-Sheet-Rich Intermediate of Lysozyme in a Solvent-Free Liquid Phase. *J. Phys. Chem. B* **2013**, *117*, 8400−8407.
(53) Arosio, P.; Rima, S.; Morbidelli, M. Aggregation Mechanism of an IgG2 and Two IgG1 Monoclonal Antibodies at Low pH: From Oligomers to Larger Aggregates. *Pharm. Res.* **2013**, *30*, 641−654.
(54) Lucas, L. H.; Ersoy, B. A.; Kueltzo, L. A.; Joshi, S. B.; Brandau, D. T.; Thyagarajapuram, N.; Peek, L. J.; Middaugh, C. R. Probing Protein Structure and Dynamics by Second-Derivative Ultraviolet Absorption Analysis of Cation-π Interactions. *Protein Sci.* **2006**, *15*, 2228−2243.
(55) Abbas, S. A.; Gaspar, G.; Sharma, V. K.; Patapoff, T. W.; Kalonia, D. S. Application of Second-Derivative Fluorescence Spectroscopy to Monitor Subtle Changes in a Monoclonal Antibody Structure. *J. Pharm. Sci.* **2013**, *102* (1), 52−61.
(56) Wen, Z.-Q. Raman Spectroscopy of Protein Pharmaceuticals. *J. Pharm. Sci.* **2007**, *96*, 2861−2878.
(57) Tuma, R. Raman Spectroscopy of Proteins: From Peptides to Large Assemblies. *J. Raman Spectrosc.* **2005**, *36*, 307−319.
(58) Tuma, R.; Thomas, G. J., Jr Theory, Design, and Characterization of a Microdialysis Flow Cell for Raman Spectroscopy. *Biophys. J.* **1996**, *71*, 3454.
(59) Tuma, R.; Prevelige, P. E.; Thomas, G. J. Mechanism of Capsid Maturation in a Double-Stranded DNA Virus. *Proc. Natl. Acad. Sci. U. S. A.* **1998**, *95*, 9885−9890.
(60) Millero, F. J.; Dexter, R.; Hoff, E. Density and Viscosity of Deuterium Oxide Solutions from 5−70.deg. *J. Chem. Eng. Data* **1971**, *16*, 85−87.
(61) Swindells, J. F. *Viscosities of Sucrose Solutions at Various Temperatures: Tables of Recalculated Values*; Supt. of Docs., U.S. G.P.O.: Washington, DC, 1958.
(62) Barnett, G. V.; Qi, W.; Amin, S.; Neil Lewis, E.; Roberts, C. J. Aggregate Structure, Morphology and the Effect of Aggregation Mechanisms on Viscosity at Elevated Protein Concentrations. *Biophys. Chem.* **2015**, *207*, 21−29.
(63) Esfandiary, R.; Hayes, D. B.; Parupudi, A.; Casas-finet, J.; Bai, S.; Samra, H. S.; Shah, A. U.; Sathish, H. A. A Systematic Multitechnique Approach for Detection and Characterization of Reversible Self-Association during Formulation Development of Therapeutic Antibodies. *J. Pharm. Sci.* **2013**, *102*, 62−72.
(64) Trappe, V.; Bauer, J.; Weissmüller, M.; Burchard, W. Angular Dependence in Static and Dynamic Light Scattering from Randomly Branched Systems. *Macromolecules* **1997**, *30*, 2365−2372.
(65) Burchard, W. Solution Properties of Branched Macromolecules. *In Branched polymers II*; Springer: New York, 1999; pp 113−194.
(66) Blanco, M. A.; Perevozchikova, T.; Martorana, V.; Manno, M.; Roberts, C. J. Protein−Protein Interactions in Dilute to Concentrated Solutions: α-Chymotrypsinogen in Acidic Conditions. *J. Phys. Chem. B* **2014**, *118*, 5817−5831.
(67) Receveur-Bréchot, V.; Durand, D. How Random Are Intrinsically Disordered Proteins? A Small Angle Scattering Perspective. *Curr. Protein Pept. Sci.* **2012**, *13*, 55.
(68) Andrews, J. M.; Roberts, C. J. A Lumry−Eyring Nucleated Polymerization Model of Protein Aggregation Kinetics: 1. Aggregation with Pre-Equilibrated Unfolding. *J. Phys. Chem. B* **2007**, *111*, 7897−7913.
(69) Witten, T. A.; Sander, L. M. Diffusion-Limited Aggregation, a Kinetic Critical Phenomenon. *Phys. Rev. Lett.* **1981**, *47*, 1400−1403.
(70) Clark, N. J.; Zhang, H.; Krueger, S.; Lee, H. J.; Ketchem, R. R.; Kerwin, B.; Kanapuram, S. R.; Treuheit, M. J.; McAuley, A.; Curtis, J. E. Small-Angle Neutron Scattering Study of a Monoclonal Antibody Using Free-Energy Constraints. *J. Phys. Chem. B* **2013**, *117*, 14029−14038.
(71) Lee, J. C.; Timasheff, S. N. The Stabilization of Proteins by Sucrose. *J. Biol. Chem.* **1981**, *256*, 7193−7201.
(72) Kendrick, B. S.; Chang, B. S.; Arakawa, T.; Peterson, B.; Randolph, T. W.; Manning, M. C.; Carpenter, J. F. Preferential Exclusion of Sucrose from Recombinant Interleukin-1 Receptor Antagonist: Role in Restricted Conformational Mobility and Compaction of Native State. *Proc. Natl. Acad. Sci. U. S. A.* **1997**, *94*, 11917−11922.

DOI: 10.1021/acs.jpcb.5b08748
J. Phys. Chem. B 2015, 119, 15150−15163

(73) Auton, M.; Bolen, D. W.; Rösgen, J. Structural Thermodynamics of Protein Preferential Solvation: Osmolyte Solvation of Proteins, Amino Acids, and Peptides. *Proteins: Struct., Funct., Genet.* **2008**, *73*, 802−813.
(74) Zhang, J.; Banks, D. D.; He, F.; Treuheit, M. J.; Becker, G. W. Effects of Sucrose and Benzyl Alcohol on GCSF Conformational Dynamics Revealed by Hydrogen Deuterium Exchange Mass Spectrometry. *J. Pharm. Sci.* **2015**, *104*, 1592−1600.

DOI: 10.1021/acs.jpcb.5b08748
J. Phys. Chem. B 2015, 119, 15150−15163